

Received February 28, 2019, accepted March 13, 2019, date of publication March 15, 2019, date of current version April 18, 2019.

Digital Object Identifier 10.1109/ACCESS.2019.2905358

# Series Arc Detection and Complex Load Recognition Based on Principal Component Analysis and Support Vector Machine

JUN JIANG<sup>1,2</sup>, ZHE WEN<sup>1</sup>, MINGXIN ZHAO<sup>1</sup>, YIFAN BIE<sup>1</sup>, CHEN LI<sup>3</sup>,  
MINGANG TAN<sup>1</sup>, AND CHAOHAI ZHANG<sup>1</sup>

<sup>1</sup>Center for More-Electric-Aircraft Power System, Nanjing University of Aeronautics and Astronautics, Nanjing 211106, China

<sup>2</sup>Jiangsu Key Laboratory of New Energy Generation and Power Conversion, Nanjing University of Aeronautics and Astronautics, Nanjing 211106, China

<sup>3</sup>State Grid Zhejiang Electric Power Co., Ltd., Research Institute, Hangzhou 310014, China

Corresponding author: Jun Jiang (jiangjun0628@nuaa.edu.cn)

This work was supported in part by the Fundamental Research Funds for the Central Universities under Grant XCA17003-04, in part by the Postgraduate Research and Practice Innovation Program of Jiangsu Province under Grant SJCX18\_0099, and in part by State Grid Zhejiang Electric Power Co., Ltd.

**ABSTRACT** The increasing household loads make series arc faults more complex, which are difficult to be detected by traditional circuit breakers and lead to the frequent occurrence of residential fire accidents. In this paper, a comprehensive approach of complex load recognition and series arc detection is proposed on the basis of principal component analysis and support vector machine (PCA-SVM) combination model. Several typical loads were selected and analyzed, especially nonlinear and complex loads like power electronics load and multi-state load. Three time-domain parameters, maximum slip difference (MSD), zero current period (ZCP) and maximum Euclidean distance (MED), and nine frequency-domain harmonics information are collected to complex waveforms. To decrease the computation cost and further to enhance the response velocity, all the time-domain and frequency-domain information were blended and dimensionally reduced to three parameters by principal component analysis (PCA). Prior to the series arc detection, load recognition is trained and completed with the artificial intelligence (AI) algorithm. At last, the comprehensive model of load recognition and series arc detection is achieved based on a support vector machine (SVM). The accuracy of load recognition and series arc detection reaches 99.1% and 99.3%, respectively, demonstrating the excellent performances of the intelligent approach to diagnose the series arcing activities in modern household applications.

**INDEX TERMS** Series arc faults, dimensionality reduction, support vector machine, load recognition, arc detection.

## I. INTRODUCTION

In U.S. alone, there are over 61,000 fires each year due to electrical failures or malfunctions on average, according to the data from the National Fire Protection Association (NFPA) [1]. Wherein, arcing and sparking in home installations are the serious hazard for residential buildings. Traditionally, fuses, Residual Current Devices (RCDs) and molded case circuits are utilized to reduce the risk of fire by detecting overcurrent or leakage current caused by failures like short circuit and parallel arc. However, they fail to eliminate series arc faults induced by loose contacts and terminals, poor connection, crushed cables, etc., since the impedance of series

The associate editor coordinating the review of this manuscript and approving it for publication was Fabio Massaro.

arc makes the load current low and difficult to be determined [2], [3]. To prevent the electrical fires, the National Electrical Code (NEC) and Underwriters Laboratories (UL) suggest arc fault circuit interrupters (AFCIs) in U.S. and International Electrotechnical Commission (IEC) [4] advises arc fault detection devices (AFDD) for household and similar uses in Europe [5].

Based on the detection of series arc fault, various algorithms and studies have been carried out to improve the accuracy and sensitivity of series arc faults. Since the time-based parameters are simple to be calculated, which was probable to be embedded and achieved in the microcontroller unit (MCU) at the early time. The relevant studies date back to the 1990s, the method of detecting arc by measuring the change of current peak was proposed [6]. Thereafter, some

algorithms based on time-domain characteristics of series arc were improved, including autocorrelation coefficient of current, crest factor, average current values and so on [7]–[9]. However, the waveforms of series arc are so complex to be distinguished that the detection accuracy of the series arc is quite low and unstable relying on the time-based parameters alone.

Owing to the development of related techniques and the improvement of hardware, two approaches have been tried to improve the detection of series arc: utilization of new sensors and signal processing methods based on frequency domain analysis. Miao *et al.* [10] used the TMR (tunnel magnetoresistance) sensor to measure the magnetic field change of the arc and calculate its power spectral density to detect the arc. Xiong *et al.* [11] used a fourth-order Hilbert fractal antenna to detect the EMR (electromagnetic radiation) signals of the arc. D-Dot sensor was also used in arc detection of switchgear [12]. Bao *et al.* [13] collected the coupling signal of high-frequency current through the transformer and calculates the high-order cumulant to detect the arc. However, these sensors are not easy to be installed and not available for manufactural and household applications. On the other hand, based on existing current measurement in the lines, high frequency information of series arc faults has been explored with various transformations and algorithms. Short Time Fourier Transformation (STFT) was used to obtain the content of fundamental wave and odd harmonic and even harmonic within 100 times [14]. Discrete Wavelet Transform (DWT) was applied to arc detection of transmission line [15]. Qi Pan *et al.* studied the influence of some parameters of wavelet transform on the accuracy of arc detection [16], [17]. Moreover, the accuracy of FFT and DWT in arc detection was compared by Wang *et al.* [18]. Instead, Artale *et al.* [19] introduced Chirp Z-Transform (CZT) and Wigner-Ville Distribution (WVD) [20] to arc detection. These methods have improved the accuracy to some extent, and high accuracy can be achieved with the rapid development of artificial intelligence (AI), including support vector machines and neural networks [21], [22]. Several characteristic quantities are extracted and trained for series arc detection, like the energy of high frequency current [23], the singular value of the improved attractor track matrix [24], sparse code [25], time-frequency gray scale images [26], etc. Nevertheless, the calculation of the smart algorithms is too complicated to embed an industrial chip. Last but not least, they have focused on the high accuracy without consideration of increasing nonlinear loads, and the applicability is still limited to traditional loads and occasions.

Since the modern loads are complexed, such as power electronics loads and multi-state loads, we considered that it is necessary to combine the load recognition and the series arc detection simultaneously with highly accurate but relatively simple calculation algorithms. Series arc detection on the complex loads is emphasized and the feature quantities are extracted in a simple and effective method. By introducing load recognition prior to arc detection, the applicability and

accuracy of the algorithm can be greatly improved. In our study, we set up an arc test platform according to the IEC 62606:2013 standard at first. Then we selected several typical loads which have individual current waveforms different from each other, especially including nonlinear loads like power electronics load and multi-state load. After the experiment, the obtained waveforms were analyzed both in time domain and frequency domain. To reduce the calculation, dimension reduction was carried out to realize feature extraction, thereafter, the featured data were inputted into artificial intelligence algorithm for model training. Finally, we got a comprehensive model of load recognition and series arc detection which can realize arc detection of high accuracy for different loads.

## II. ARC EXPERIMENT AND DATA PROCESSING

### A. ARCING FAULT GENERATION

The arc experiment platform has been designed as shown in Fig. 1. Arc generator is designed according to IEC 62606:2013 standard, it includes a base and two electrodes, one electrode consists of a  $6\text{ mm} \pm 0.5\text{ mm}$  diameter carbon-graphite rod and the other electrode is a copper rod. The type of other devices is listed below.

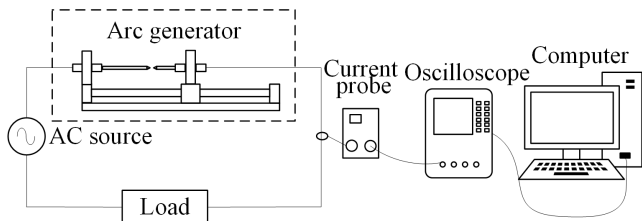


**FIGURE 1.** Experimental setup of series arc fault.

Current probe: type: TCP303 and TCPA300, produced by Tektronix;

Oscilloscope: type: MDO 3034, produced by Tektronix.

The bandwidth of the current probe is 0-15 MHz, and the accuracy is  $\pm 1\%$ . The lowest measurable current (at  $\pm 3\%$  accuracy at DC) is 5 mA. The bandwidth of the oscilloscope is 0-500 MHz, the maximum sampling rate of a single channel is 2.5 GS/s.

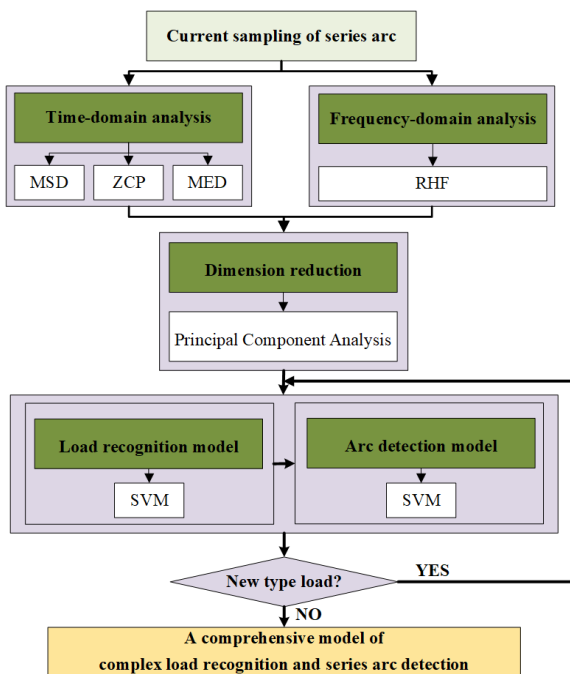
There are countless household loads, but the waveforms of the same kind of loads have extremely similar characteristics, both in time domain and frequency domain. Therefore, we selected four typical loads for the experiment, the power of each loads are given in Table 1. The oscilloscope is connected to a computer and controlled by LabVIEW. In this way, a good deal of waveforms can be saved quickly and automatically.

### B. IMPLEMENTATION STRATEGY

Based on the established arc experiment platform and the typically selected loads, our overall scheme is shown in the Fig. 2. The method based on time domain is easy to be calculated and represents good accuracy in some loads.

**TABLE 1.** Type and power parameters of the selected loads.

NO.	Load	Power	Type
1	Bulb	100W	Linear load
2	LED light	5W	Power electronic load
3	Fan	20W	Nonlinear load
4	Electric soldering iron	50W	Multi-state load

**FIGURE 2.** Load recognition and arc detection strategy based on dimensionality reduction method and artificial intelligence algorithm.

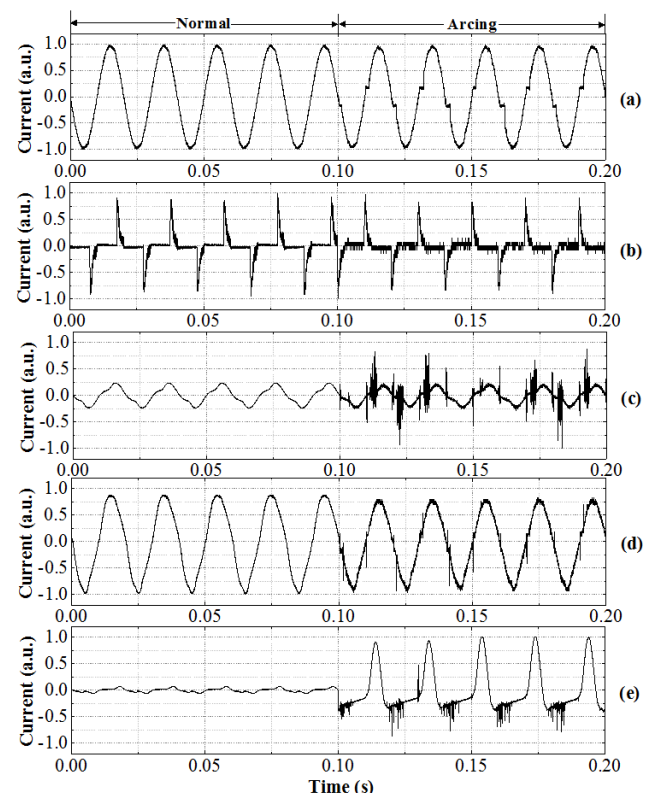
Therefore, we extracted the following three characteristic quantities to describe the time-domain information of different loads: Maximum Slip Difference (MSD), Zero Current Period (ZCP) and Maximum Euclidean Distance (MED). At the same time, it is necessary to obtain more details and information of loads and possible series arcing phenomenon on the basis of frequency domain. It is no doubt that the more time and frequency domain parameters are considered comprehensively, the more accurate for the determination of the series arc. However, it requires a large amount of computational cost and response time with the consideration of a number of time domain calculation and frequency domain analysis, and the calculation efficiency is difficult to be guaranteed. To solve the problem, we utilize Principal Component Analysis (PCA) as the dimensionality reduction method to retain the original information commendable. Thereafter, artificial intelligence algorithms, Back Propagation Neural Networks (BPNN) and Support Vector Machine (SVM), are selected and compared for the load identification

and arc detection. It should be mentioned that the model can continue to learn and expand. When new load types appear, the model will be retrained for further refinement, and the type will be marked in the characteristic quantities after dimension reduction.

### C. TIME-DOMAIN ANALYSIS

The sampling frequency adopted in this experiment is 100 kHz, and the sampling period is  $T = 5$ , so each period has  $k = 2000$  points and  $n = 10,000$  points in total. Each load was collected 200 sets of waveforms, and we collected  $N=800$  sets of waveforms in the end. By sampling plenty of waveforms, the influence of randomness of arcs can be reduced.

The current waveforms of the different loads in normal and arcing are shown in Fig. 3. In order to evaluate the difference between normal waveform and arc fault waveform, all data were normalized in arbitrary unit (a.u.). We set the maximum value of the absolute value of the current as 1 and divide the current value of the rest of the points in the sample by the maximum value. Electric soldering iron has two working states: heating mode and constant temperature mode, which leads to five different waveforms in four loads.

**FIGURE 3.** The normalized current waveforms of typical loads with series arc. (a) Bulb, (b) LED light, (c) fan, (d) electric soldering iron (heating mode), (e) electric soldering iron (constant temperature mode).

The current waveform of the bulb in the arc fault exists the “flat shoulder”, which means the current fluctuates near zero period. However, the current value and length of the

“flat shoulder” are random. There is a significantly increase of the current amplitude in fan and electric soldering iron (constant temperature mode) whereas other loads show obvious increase of higher harmonics. Due to the energy storage components (mainly inductance), temperature detection module and the temperature control module in the soldering iron, the noisy segments in constant temperature mode witnesses the occurrence of series arc.

Firstly, the Maximum Slip Difference (MSD) was used to characterize the abrupt change of current. Both the high-order harmonics and the changes of current at the head and tail of the “flat shoulder” can be well reflected by this value. The current value of each sampling point was denoted as  $I_n$ , and the sliding window size was selected as 10. The equation is shown below:

$$MSD = \max \left| \left( \sum_{i=1}^{i+4} I_i - \sum_{i=5}^{i+9} I_i \right) / 5 \right| \quad (i = 1, 2, \dots, n-9) \quad (1)$$

Secondly, the Zero Current Period (ZCP) of the waveform was calculated. We took the absolute value of the sampling current and a tenth of the maximum value was regarded as the threshold. Both MSD and ZCP can get the correct value when the sampling covers more than a single period. In order to ensure the consistency of the calculation, the five cycles were included in the calculation and the maximum value was obtained.

In normal operation, the waveform of different loads is unique, but adjacent period of the waveform of single load shows a high degree of similarity. In the case of arc fault, due to the randomness of the arc, adjacent period of the waveform become dissimilar. Therefore, we chose the Maximum Euclidean Distance (MED) as the characteristic quantity to measure the similarity of adjacent periods. The equation is shown below:

$$MED = \max \left( \sqrt{\sum_{i=1}^k (I_i^T - I_{i+1}^{T+1})^2} \right) \quad (T = 1, 2, 3, 4) \quad (2)$$

$T$  should be less than 5 in this equation because it is the corresponding current value of the adjacent period. For the 800 set of waveforms obtained by sampling, three time-domain characteristics were calculated respectively, as shown in Fig. 4.

#### D. FREQUENCY-DOMAIN ANALYSIS

The most commonly used spectrum analysis method is the Fourier Transform (FT). In practical applications, continuous signals are sampled into discrete signals, so the spectrum can be calculated by Discrete Fourier Transform (DFT). As mentioned above, the sampling frequency set by the experiment is 100 kHz, and the number of sampling points is 10000 points, therefore the frequency resolution is 10 Hz. Sampling is synchronized so there is no spectrum leakage, and the spectrum information is accurately obtained. The integral harmonic content of both normally working and series arcing condition less than 10 times is shown in Fig. 5.

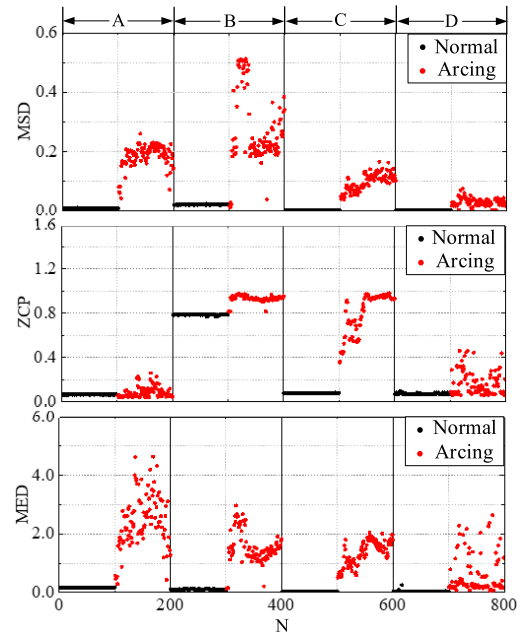


**FIGURE 4.** The time domain characteristic quantities of different typical loads. (A) Bulb, (B) LED light, (C) fan, (D) electric soldering iron (heating mode and constant temperature mode).

When the arc fault occurs, the harmonic content changes of different loads are not consistent, which further proves the importance of load recognition. For the bulb load, the fundamental wave content decreases and the harmonic content increases. For the LED load, the even harmonic content increases obviously. As for the electric soldering iron (constant temperature mode), the fundamental wave content and the first 5 harmonics content increase significantly, which is consistent with the waveform performance in Fig. 3(e).

### III. LOAD RECOGNITION AND ARC DETECTION

#### A. PRINCIPAL COMPONENT ANALYSIS

With these time-domain and frequency-domain characteristic information, the load type and running status corresponding to each waveform were uniquely determined. Principal Component Analysis was utilized to obviously reduce the calculation cost, under the premise of ensuring the accuracy of calculation.

PCA is a statistical method that transforms a set of correlated variables into a set of unrelated variables by orthogonal transformation. We have  $N=800$  sets of current waveforms, and the characteristic information of each set of waveforms has  $D=12$  dimensions: 3 time-domain information and 9 frequency-domain information. To begin with, the mean of each column of data was calculated and subtracted from the corresponding column data. Then the data make up the sample matrix  $X$ . We want to find a low dimensional projection space  $W$  that maximizes the variance  $\lambda$  of the projected sample points.  $\lambda$  is:

$$\lambda = \frac{1}{D} \sum_{i=1}^D (x_i^T \omega)^2 \quad (3)$$

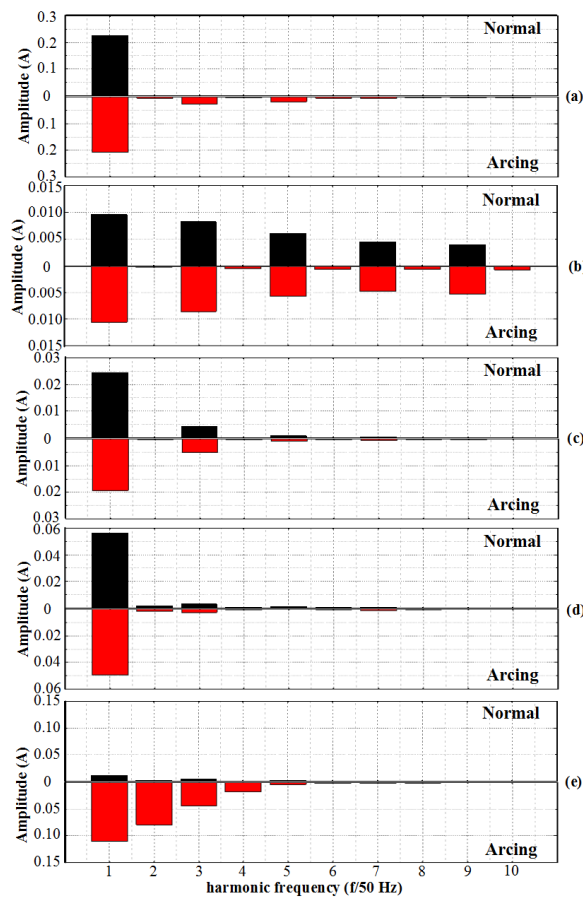


**FIGURE 5.** The FFT results of different typical loads. (a) Bulb, (b) LED light, (c) fan, (d) electric soldering iron (heating mode), (e) electric soldering iron (constant temperature mode).

where,  $\omega$  is the axial vector projected onto the space  $W$ .  $x_i$  is the column vector of sample matrix  $X$ . After the transformation:

$$\lambda = \frac{1}{D} \omega^T \sum_{i=1}^D (x_i x_i^T) \omega = \frac{1}{D} \omega^T X X^T \omega \quad (4)$$

$\frac{1}{D} X X^T$  is the covariance matrix  $Y$  of the sample matrix  $X$ . So the original equation is equal to:

$$\omega \lambda = Y \omega \quad (5)$$

$\lambda$  is the eigenvector of the covariance matrix  $Y$ . If we want the maximum total variance after projection, we need calculate the largest  $\lambda$ , and the eigenvector corresponding to  $\lambda$  is the first principal component. On the analogy of this, we can get the second eigenvector, the third eigenvector, and so on.

After the eigenvector was obtained, the eigenmatrix was constructed, and then the mixed information matrix of both domain and frequency domain was multiplied to obtain the principal component matrix. The result is shown in Table 2.

**TABLE 2.** The principal component matrix after dimension reduction of PCA.

NO.	C1	C2	C3
1	-0.69766	-0.42126	0.02908
2	-0.70122	-0.42034	0.02925
3	-0.70003	-0.42173	0.03013
4	-0.70075	-0.41996	0.02903
5	-0.70298	-0.42055	0.0288
6	-0.702	-0.42094	0.0292
...	...	...	...
798	-0.71186	-0.3913	0.00912
799	0.32489	-0.48843	-0.02499
800	-0.71346	-0.38394	0.01141

The proportion of original information can be represented by the characteristic contribution rate. The value of these three columns of principal components are shown in Table 3.

**TABLE 3.** The characteristic contribution rate of the principal components (%).

Principal components	C1	C2	C3	Total
Contribution rate	70.4	24.9	2.2	97.5

It is observed that the characteristic contribution rate of these three columns of principal components reached 97.5%, which shows that the original information has been retained well. The result is drawn as a three-dimensional feature scatter diagram for 4 different loads as shown in Fig. 6.

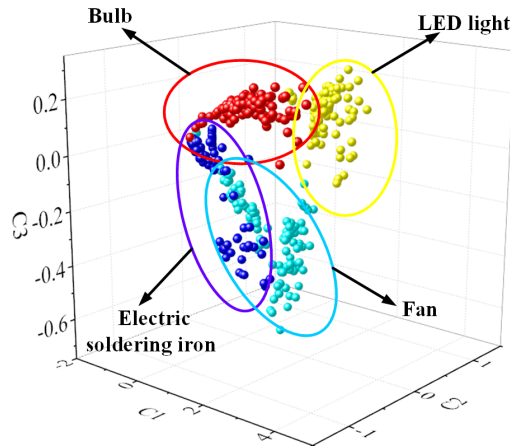


**FIGURE 6.** The characteristic scatter diagram drawn by the three-dimensional principal components.

## B. LOAD RECOGNITION

Back Propagation Neural Networks (BPNN), which is the most commonly used in machine learning, is introduced to carry out the load recognition in our study. The basic structure

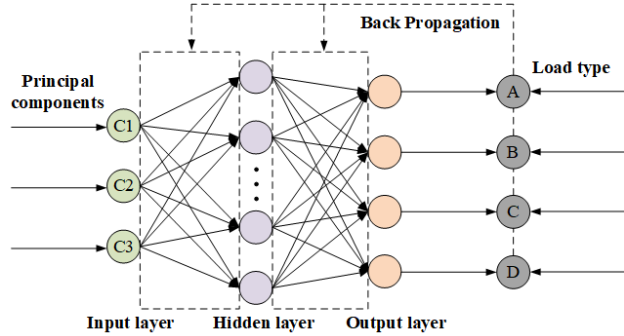


**FIGURE 7.** The structure and training process of three-layer BPNN for load recognition.

and training process of BPNN usually consists of an input layer, a hidden layer, and an output layer, as shown in Fig. 7. Each layer consists of several neurons. The input layer contained three neurons corresponding to the three principal components obtained after dimension reduction. The number of neurons in the output layer was 4, consistent with the load type. The number of hidden layer neurons was determined by equation (6).  $HL$ ,  $IL$ , and  $OL$  are the number of neurons in hidden layer, input layer and output layer respectively.  $c$  is a constant between 5 and 10.

$$HL = \sqrt{IL + OL} + c \quad (6)$$

There is a gap between the models trained by different number of neurons. The learning rate and the number of iterations, and so on, will also have an impact on the results. The training of BPNN includes two processes, the forward propagation of signal and the back propagation of error. In other words, when the output layer is inconsistent with the expected output, the error is calculated and the parameters of the neural network of each layer are changed according to back propagation.

Determining the optimal parameters, we got the load identification model based on BPNN. The confusion matrix was obtained in Fig. 8. The accuracy of load identification reached 98.8% at the most. However, the parameters have a great impact on the BPNN model, and the learning rate is slow, so it is easy to fall into the local minimum without obtaining the optimal solution [27], [28].

Based on the above problems, we further explored the possibility of Support Vector Machine (SVM) as a load identification method. SVM has been ported to Digital Signal Processor (DSP) to implement the construction of various systems [29]. Due to the remarkable dimension reduction previously, the data acquisition and signal processing are able to be performed well in a single DSP chip within several milliseconds.

SVM is a dichotomous model with supervised learning. Given a train set, a hyperplane is searched through model training. SVM would judge whether the new samples belong to this class or other classes. The linear equation describing

Output Class	Target Class				Overall Accuracy
	1	2	3	4	
1	200 25.0%	0 0.0%	0 0.0%	1 0.1%	99.5% 0.5%
2	0 0.0%	200 25.0%	0 0.0%	0 0.0%	100% 0.0%
3	0 0.0%	0 0.0%	193 24.1%	2 0.3%	99.0% 1.0%
4	0 0.0%	0 0.0%	7 0.9%	197 24.6%	96.6% 3.4%
	100% 0.0%	100% 0.0%	96.5% 3.5%	98.5% 1.5%	98.8% 1.2%

**FIGURE 8.** The structure and training process of three-layer BPNN for load recognition.

the hyperplane is:

$$f(x) = z^T x + b \quad (7)$$

In which,  $z$  is the normal vector of the hyperplane, which determines the direction of the hyperplane;  $b$  is the displacement of the hyperplane, which determines the distance between the hyperplane and the origin. For the training sample  $(x_i, y_i)$ , it satisfies:

$$\begin{aligned} z^T x_i + b &\geq +1 (y_i = +1) \\ z^T x_i + b &\leq -1 (y_i = -1) \end{aligned} \quad (8)$$

+1 means that the sample is a positive sample, which belongs to this class, and -1 means a negative sample, which does not belong to this class. So this expression can be converted to:

$$y_i (z^T x_i + b) \geq 1 \quad (9)$$

A sample that satisfies the equality relationship is called “support vector”. To maximize the projection spacing of the support vector on the hyperplane, we get the following constraint:

$$\begin{aligned} \min_{z, b} \frac{1}{2} \|z\|^2 \\ \text{s.t. } y_i (z^T x_i + b) \geq 1 \quad (i = 1, 2 \dots n) \end{aligned} \quad (10)$$

Kernel function  $k(x_i, y_i)$  is introduced to realize nonlinear classification. After derivation and transformation, the constraint is converted to:

$$\begin{aligned} \max_{\alpha} \sum_{i=1}^n \alpha_i - \frac{1}{2} \sum_{i=1}^n \sum_{j=1}^n \alpha_i \alpha_j y_i y_j k(x_i, x_j) \\ \text{s.t. } \sum_{i=1}^n \alpha_i y_i = 0, \quad \alpha_i \geq 0, \quad i=1, 2 \dots n \end{aligned} \quad (11)$$

$\alpha$  is the Lagrange multiplier, the final hyperplane equation is:

$$f(x) = \sum_{i=1}^n \alpha_i y_i k(x_i, x_j) + b \quad (12)$$

There are many kinds of kernel functions, finally we decided to use the Gaussian kernel, owing to its excellent nonlinear fitting ability.

Two columns of principal components were selected for training at first, since less parameter input leads to less computation and thus faster response time. The results of the model are shown in the Fig. 9.

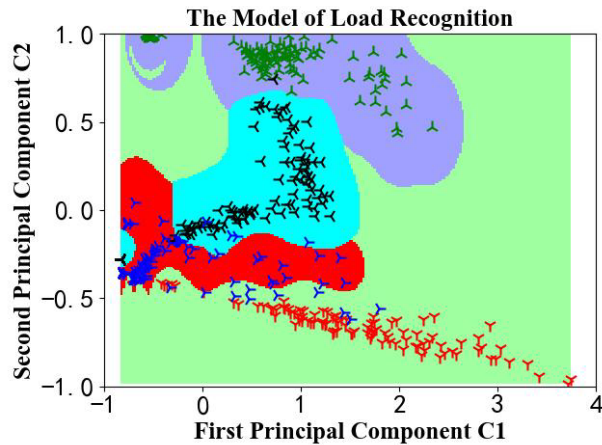


**FIGURE 9.** The load recognition model trained by two-dimensional principal component (Green zone-bulb, Purple zone-LED light, Cyan zone-fan, Red zone-electric soldering iron).

In this case, the load recognition accuracy reached 95.3%, which could be further promoted. Furthermore, all the principal components of the three columns were input to the SVM for training, and the load recognition accuracy reached 99.1% at last. Therefore, the use of PCA-SVM has the advantage of high accuracy and small computation, and avoids the disadvantages of BPNN. It is a suitable approach for the complex load recognition.

### C. SERIES ARC DETECTION

In our study, we do think it is extremely important to separate the load type prior to series arc detection and identification instead of direct determination of the arc fault on the basis of current measurement. After realizing load identification, arc detection is liberated from complex loads and then we could focus on the operation of single load. The principal components obtained by PCA were trained again, then we obtained the arc detection model of different loads. Similarly, the model of arc detection trained by two-dimensional principal component, as shown in Fig. 10. Normal waveform was very concentrated after dimension reduction, whereas the arc fault waveform was obviously disordered due to the randomness of arcing activities.

The arc detection accuracy of different loads was shown in Table 4. With only two principal components, the accuracy

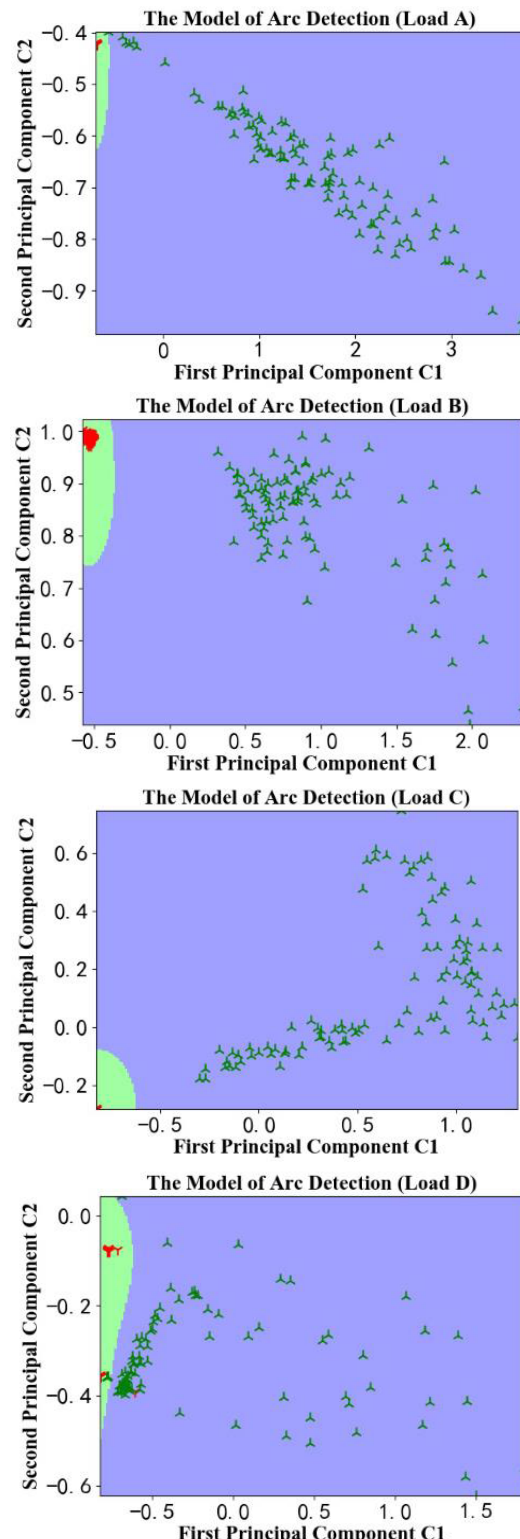


**FIGURE 10.** The load recognition model trained by two-dimensional principal component (Green zone-bulb, Purple zone-LED light, Cyan zone-fan, Red zone-electric soldering iron).

of arc detection model reached 99.3%, and the accuracy of electric soldering iron, which has two working mode, reached 97.0% as well. When the third principal component was

**TABLE 4.** Arc detection accuracy of different loads based on SVM.

Load	Test set size	Wrong quantities	Accuracy
Bulb	100	0	100.0%
LED light	100	0	100.0%
Fan	100	0	100.0%
Electric soldering iron	100	3	97.0%
Total	400	3	99.3%

added, the accuracy was not obviously improved. Therefore, the training of arc detection model could be realized based on two principal components, which greatly reduced the computation. The high accuracy and applicability of the method has been verified based on the SVM algorithm.

#### IV. CONCLUSION

To be brief, we report a comprehensive approach of complex load recognition and series arc detection model in this paper instead of conventional arc detection methods. Based on principal component analysis and support vector machine (PCA-SVM) combination algorithm, following advantages have been achieved.

(1) High accuracy. Artificial intelligence algorithms, BPNN and SVM, are emphasized and compared. With the application of Gaussian kernel, SVM is proved to less computation, higher accuracy and faster response time. Load recognition and series arc detection are achieved simultaneously, and the accuracy of load recognition and arc detection reaches 99.1% and 99.3%, respectively.

(2) Strong applicability. Different from existing work, load identification is introduced and a variety of complex loads are selected in the experiment, especially the multi-state load and power electronics loads have been emphasized and considered. All the typical loads prove to be well recognized and detected.

(3) Good portability. A total of 12 columns of information are considered and calculated in time-domain and frequency-domain simultaneously, and only 3 columns of principal components are obtained by PCA. The original information is fully retained, and the calculation amount and the setting of redundant parameters are significantly reduced.

Further research will be focused on the expansion of more loads and long-term reliability of the series arc monitoring system.

#### ACKNOWLEDGMENT

The authors feel gratitude for the comments of Dr. Ricardo Albaracín from Universidad Politécnica de Madrid.

#### REFERENCES

- [1] National Fire Protection Association (NFPA). Accessed: Mar. 15, 2018. [Online]. Available: <https://www.nfpa.org>
- [2] F. M. Uriarte *et al.*, “A DC arc model for series faults in low voltage microgrids,” *IEEE Trans. Smart Grid*, vol. 3, no. 4, pp. 2063–2070, Dec. 2012.
- [3] Y. Wang, F. Zhang, X. Zhang, and S. Zhang, “Series AC arc fault detection method based on hybrid time and frequency analysis and fully-connected neural network,” *IEEE Trans. Ind. Informat.*, to be published. doi: [10.1109/TII.2018.2885945](https://doi.org/10.1109/TII.2018.2885945).
- [4] *General Requirements for Arc Fault Detection Devices*. IEC Standard 62606, 2013.
- [5] C. J. Wu and Y. W. Liu, “Smart detection technology of serial arc fault on low-voltage indoor power lines,” *Int. J. Electr. Power Energy Syst.*, vol. 69, pp. 391–398, Jul. 2015.
- [6] A. F. Sultan, G. W. Swift, and D. J. Fedirchuk, “Detecting arcing downed-wires using fault current flicker and half-cycle asymmetry,” *IEEE Trans. Power Del.*, vol. 9, no. 1, pp. 461–470, Jan. 1994.
- [7] J. Lezama, P. Schweitzer, S. Weber, E. Tisserand, and P. Joycux, “Arc fault detection based on temporal analysis,” in *Proc. IEEE 60th Holm Conf. Elect. Contacts*, Oct. 2014, pp. 1–5.
- [8] J. Lezama, P. Schweitzer, E. Tisserand, J.-B. Humberta, S. Webara, and P. Joyeux, “An embedded system for AC series arc detection by inter-period correlations of current,” *Electr. Power Syst. Res.*, vol. 129, pp. 227–234, Dec. 2015.
- [9] S. Zhang, F. Zhang, P. Liu, and Z. Han, “Identification of low voltage AC series arc faults by using Kalman filtering algorithm,” *Elektron. Elektrotech.*, vol. 20, no. 5, pp. 51–56, 2014.
- [10] W. Miao, X. Liu, K. H. Lam, and P. W. T. Pong, “DC-Arcing Detection by Noise Measurement With Magnetic Sensing by TMR Sensors,” *IEEE Trans. Magn.*, vol. 54, no. 11, Nov. 2018, Art. no. 4002005.
- [11] Q. Xiong *et al.*, “Electromagnetic radiation characteristics of series dc arc fault and its determining factors,” *IEEE Trans. Plasma Sci.*, vol. 46, no. 11, pp. 4028–4036, Nov. 2018.
- [12] G. A. Hussain, M. Shafiq, M. Lehtonen, and M. Hashmi, “Online condition monitoring of MV switchgear using D-dot sensor to predict arc-faults,” *IEEE Sensors J.*, vol. 15, no. 12, pp. 7262–7272, Dec. 2015.
- [13] G. Bao, R. Jiang, and D. Liu, “Research on series arc fault detection based on higher-order cumulants,” *IEEE Access*, vol. 7, pp. 4586–4597, 2018. doi: [10.1109/ACCESS.2018.2888591](https://doi.org/10.1109/ACCESS.2018.2888591).
- [14] H. Cheng, X. Chen, F. Liu, and C. Wang, “Series arc fault detection and implementation based on the short-time fourier transform,” in *Proc. Asia-Pacific Power Energy Eng. Conf.*, Mar. 2010, pp. 1–4.
- [15] C.-H. Kim, H. Kim, Y.-H. Ko, S.-H. Byun, R. K. Aggarwal, and A. T. Johns, “A novel fault-detection technique of high-impedance arcing faults in transmission lines using the wavelet transform,” *IEEE Trans. Power Del.*, vol. 17, no. 4, pp. 921–929, Oct. 2002.
- [16] P. Qi, S. Jovanovic, J. Lezama, and P. Schweitzer, “Discrete wavelet transform optimal parameters estimation for arc fault detection in low-voltage residential power networks,” *Electric Power Syst. Res.*, vol. 143, pp. 130–139, Feb. 2017.
- [17] H.-K. Ji, G. Wang, W.-H. Kim, and G.-S. Kil, “Optimal design of a band pass filter and an algorithm for series arc detection,” *Energies*, vol. 11, no. 4, p. 992, 2018. doi: [10.3390/en11040992](https://doi.org/10.3390/en11040992).
- [18] Z. Wang, S. McConnell, R. S. Balog, and J. Johnson, “Arc fault signal detection-Fourier transformation vs. wavelet decomposition techniques using synthesized data,” in *Proc. IEEE 40th Photovoltaic Spec. Conf. (PVSC)*, Jun. 2014, pp. 3239–3244.
- [19] G. Artale, A. Cataliotti, V. Cosentino, D. Di Cara, S. Nuccio, and G. Tiné, “Arc fault detection method based on CZT low-frequency harmonic current analysis,” *IEEE Trans. Instrum. Meas.*, vol. 66, no. 5, pp. 888–896, May 2017.
- [20] J. Liu, K. Zhou, and Y. Hu, “EMD-WVD method based high-frequency current analysis of low voltage arc,” in *Proc. Condition Monitor. Diagnosis (CMD)*, Sep. 2018, pp. 1–5.
- [21] J. E. Siegel, S. Pratt, Y. Sun, and S. E. Sarma, “Real-time deep neural networks for internet-enabled arc-fault detection,” *Eng. Appl. Artif. Intell.*, vol. 74, pp. 35–42, Sep. 2018.
- [22] Y.-W. Liu, C.-J. Wu, and Y.-C. Wang, “Detection of serial arc fault on low-voltage indoor power lines by using radial basis function neural network,” *Int. J. Electr. Power Energy Syst.*, vol. 83, pp. 149–157, Dec. 2016.
- [23] K. Yang, R. Zhang, J. Yang, C. Liu, S. Chen, and F. Zhang, “A novel arc fault detector for early detection of electrical fires,” *Sensors*, vol. 16, no. 4, p. 500, 2016. doi: [10.3390/s16040500](https://doi.org/10.3390/s16040500).
- [24] H. Gao *et al.*, “Research on feature of series arc fault based on improved SVD,” in *Proc. IEEE Holm Conf. Elect. Contacts*, Sep. 2017, pp. 325–331.
- [25] Y. Wang, F. Zhang, and S. Zhang, “A new methodology for identifying arc fault by sparse representation and neural network,” *IEEE Trans. Instrum. Meas.*, vol. 67, no. 11, pp. 2526–2537, Nov. 2018. doi: [10.1109/TIM.2018.2826878](https://doi.org/10.1109/TIM.2018.2826878).

- [26] M.-F. Guo, X.-D. Zeng, D.-Y. Chen, and N.-C. Yang, "Deep-learning-based earth fault detection using continuous wavelet transform and convolutional neural network in resonant grounding distribution systems," *IEEE Sensors J.*, vol. 18, no. 3, pp. 1291–1300, Feb. 2017.
- [27] D. Niu, Y. Liang, H. Wang, M. Wang, and W.-C. Hong, "Icing forecasting of transmission lines with a modified back propagation neural network-support vector machine-extreme learning machine with Kernel (BPNN-SVM-KELM) based on the variance-covariance weight determination method," *Energies*, vol. 10, no. 2, p. 1196, 2017. doi: [10.3390/en10081196](https://doi.org/10.3390/en10081196).
- [28] Y. Q. Ni and M. Li, "Wind pressure data reconstruction using neural network techniques: A comparison between BPNN and GRNN," *Measurement*, vol. 88, pp. 468–476, Jun. 2016.
- [29] G. Shi, C. S. Chan, W. J. Li, K.-S. Leung, Y. Zou, and Y. Jin, "Mobile human airbag system for fall protection using MEMS sensors and embedded SVM classifier," *IEEE Sensors J.*, vol. 9, no. 5, pp. 495–503, May 2009.

Authors' photographs and biographies not available at the time of publication.

• • •